ACS chemical biology

pubs.acs.org/acschemicalbiology

Letters

Selectively Disrupting m^{6}A-Dependent Protein−RNA Interactions with Fragments

Rajiv Kumar Bedi, Danzhi Huang, Lars Wiedmer, Yaozong Li, Aymeric Dolbois, Justyna Aleksandra Wojdyla, May Elizabeth Sharpe, Amedeo Caflisch,* and Pawel Sledz*

Cite This: *ACS Chem. Biol.* 2020, 15, 618−625

Read Online

ACCESS | Metrics & More | Article Recommendations | Supporting Information

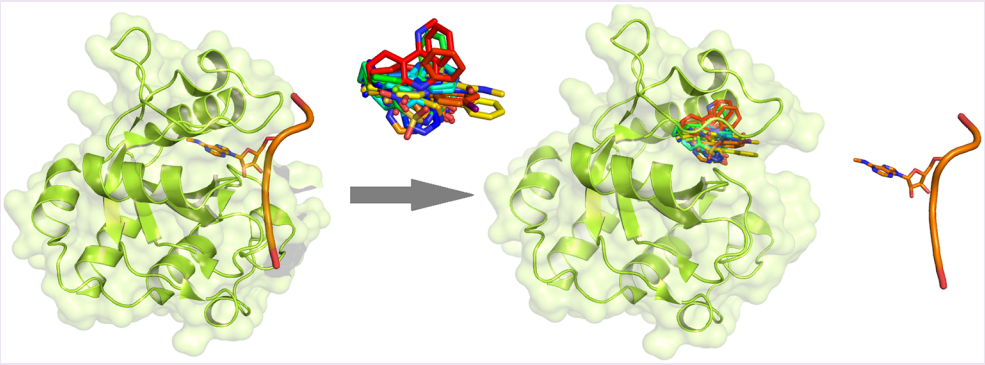

ABSTRACT: We report a crystallographic analysis of small-molecule ligands of the human YTHDC1 domain that recognizes N6-methylated adenine (m^{6}A) in RNA. The 30 binders are fragments (molecular weight < 300 g mol^{-1}) that represent 10 different chemotypes identified by virtual screening. Despite the structural disorder of the binding site loop (residues 429−439), most of the 30 fragments emulate the two main interactions of the −NHCH$_3$ group of m^{6}A. These interactions are the hydrogen bond to the backbone carbonyl of Ser378 and the van der Waals contacts with the tryptophan cage. Different chemical groups are involved in the conserved binding motifs. Some of the fragments show favorable ligand efficiency for YTHDC1 and selectivity against other m^{6}A reader domains. The structural information is useful for the design of modulators of m^{6}A recognition by YTHDC1.

Protein−RNA interactions play an important role in regulation of gene expression and contribute to a range of events relevant to normal development as well as to pathological conditions. Usually, the recognition of RNA by the protein binders predicates on polar interactions to recognize the bases and on salt bridges to attract the phosphate backbone. Therefore, protein−RNA interfaces usually lack hydrophobic druggable pockets that could be targeted with small molecules. This is reflected by lack of small molecule therapeutics acting by disrupting interactions between proteins and RNA, with only the first example, H3B-8800[1] modulating the interactions of spliceosome subunit SF3B1, being awarded the orphan drug status in 2017 and undergoing clinical studies in leukemia.

Recent years have witnessed developments in hit finding methodologies and expansion of the target space tractable by small molecule therapeutic approaches. Many protein−protein interactions, a "high hanging fruit" target class often characterized by flat and featureless interfaces, were successfully targeted either in high throughput screening efforts or by biophysics- and structural-biology-driven fragment-based approaches. More recently, examples of small molecules that can directly bind structured RNA have emerged.[2] These breakthroughs were enabled by target selection efforts and better understanding of molecular recognition of these target classes, which reveal more and more binding pockets that could be suitable for small molecule binding. Examples include RNA structures that naturally bind small molecules (e.g., riboswitches) or protein−protein interfaces that bind peptide chains in their extended conformation and feature binding pockets recognizing individual side chains.

To date, more than 150 epitranscriptomic (i.e., posttranscriptional) modifications of RNA have been discovered and demonstrated to play important roles in processes relevant to life and disease. For example, the most prevalent modification, methylation of position N6 in adenine (the m^{6}A modification), affects the secondary and tertiary structure of the RNA chain and its ability to form protein−RNA interactions and thus

Received: November 4, 2019
Accepted: February 26, 2020
Published: February 26, 2020

https://dx.doi.org/10.1021/acschembio.9b00894
ACS Chem. Biol. 2020, 15, 618−625

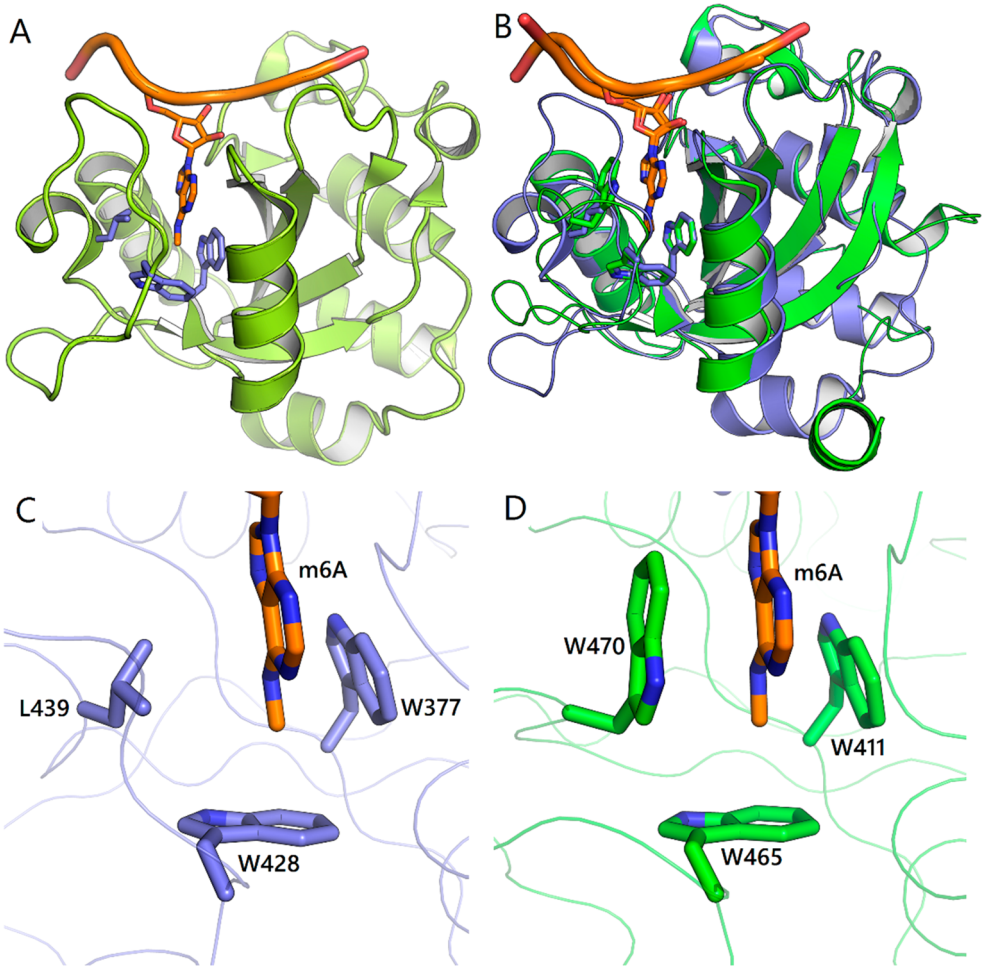

Figure 1. Aromatic/aliphatic cage for m^{6}A recognition. (A) Structure of the YTH domain of YTHDC1 (olive, side chains in violet) in complex with oligoribonucleotide containing m^{6}A (orange) (PDB code 4R3I). (B) Structural overlap of YTHDC1 (blue) and YTHDF1 (green). (C) Binding pocket of m^{6}A in YTHDC1 (PDB code 4R3I). (D) Binding pocket of m^{6}A in YTHDF1 (PDB code 4RCJ).

modulates the processing, translation, and stability of transcripts.[3] In consequence, m^{6}A is implicated in controlling embryonic development processes and stem cell differentiation, regulating the mammalian circadian clock and modulating stress response, e.g., heat shock. The malfunctions of the cellular machinery regulating the m^{6}A modification have been linked to pathologies like obesity, cancer, and neurodegeneration. Therefore, the m^{6}A modification machinery has recently attracted broad attention from the drug discovery community.[4,5] Importantly, the molecular recognition and physicochemical properties of RNA change upon its posttranscriptional covalent modifications. In the case of m^{6}A modification, the base becomes more hydrophobic.[6] The corresponding reader proteins (i.e., proteins that specifically recognize the modification to elicit cellular response to it)[7] feature a binding pocket [Figure 1A] that is more hydrophobic than the interfaces that bind unmodified RNA.[8] Thus, this pocket is likely to be more amenable to small molecule intervention. It should be noted that a similar observation has been made for bromodomains, the protein modules that specifically bind acetylated lysine, demonstrated as robust targets for small molecule binding.[9] It is reasonable to assume that a pocket recognizing unmodified lysine would be more polar than the bromodomain pocket, and likely recalcitrant to small molecule binding.

There are five direct readers of the m^{6}A modification in the human genome and each of them contains one YTH domain.[10] The aromatic hydrophobic cage is the key to specific recognition of m^{6}A modification [Figure 1]. The YTH domain-containing readers YTHDF1, YTHDF2, and YTHDF3 have three Trp side chains that specifically recognize the partial positive charge on the methyl group through the π−cation type of interactions [Figure 1D]. Some YTH domains feature a noncanonical Trp cage; e.g., one of the Trp residues is replaced by another aromatic residue (like tyrosine in the case of fungal homologue MRB1) or an aliphatic side chain like leucine in the case of human nuclear reader YTHDC1 [Figure 1C].[11]

In this paper, we dissect the chemical space of ligands that can mimic epitranscriptomic m^{6}A modification of mRNA. Our computational screening of fragments[12−16] has revealed 10 diverse chemotypes to occupy the recognition site of m^{6}A. We show that such epitranscriptomic-dependent protein−RNA interaction sites can be druggable and propose a range of chemical moieties (including both aliphatic and aromatic chemical groups) that can be used as isosteres of this epitranscriptomic modification. We also describe in detail the common features shared by most identified YTH domain binders as well as explore opportunities presented by conformational changes of the protein to accommodate ligands

https://dx.doi.org/10.1021/acschembio.9b00894
ACS Chem. Biol. 2020, 15, 618−625

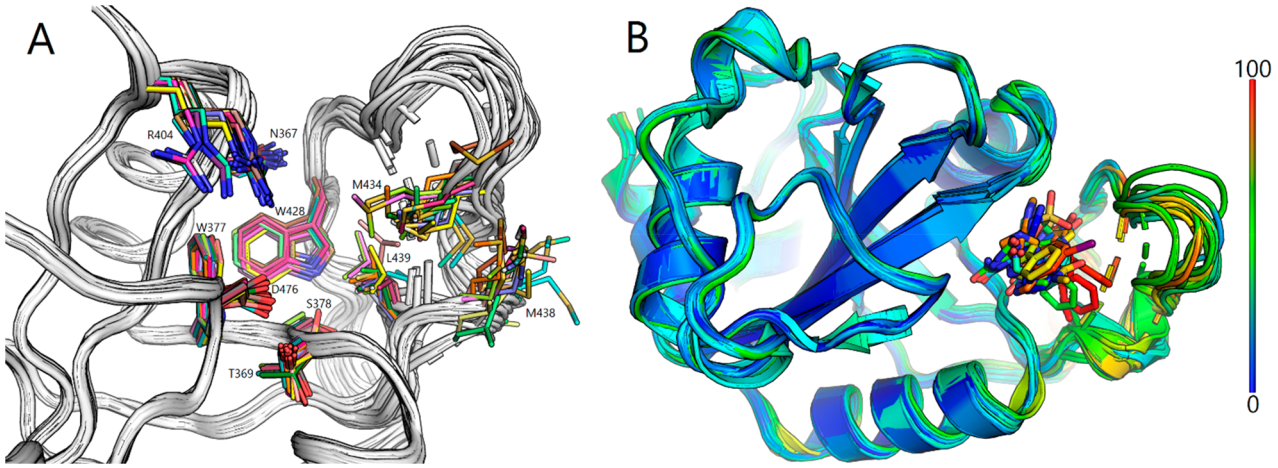

Figure 2. Binding site and loop flexibility in the 30 crystal structures of the holo m^{6}A reader domain of YTHDC1. The structural overlap was carried out using the Cα atoms. PDB codes of the 30 structures are listed in Table 1. (A) Side chains in the m^{6}A binding pocket. The 30 fragments are not shown. (B) Structural overlap of the backbone colored according to crystallographic B factors (from blue to red). Broken segments of the loop indicate lack of electron density. The 30 fragments are shown in different colors.

[Figure 2]. Finally, we propose *N*-methyl amides as particularly interesting scaffolds to further explore molecular recognition of the binding site.

To study the molecular recognition of YTH domains, we selected YTHDC1, a direct nuclear YTH domain-containing reader, involved in splicing regulation and exportation. We used high-throughput docking[12−14] as a primary screening methodology. More precisely, libraries of rigid fragments were docked with the program SEED,[12,13] while AutoDock[17] and a function that penalizes unsatisfied polar groups[14] were employed for flexible molecules. The structure of YHTDC1 was considered rigid during docking and evaluation of binding energy. Both SEED and AutoDock calculate the binding energy by a force field with implicit treatment of the electrostatics effects of the solvent. Fragment screening by SEED requires about 1 s per fragment. SEED is available as an open source code from GitLab (https://gitlab.com/CaflischLab). Docking by AutoDock requires about 1 min or more per molecule depending on the flexibility of the ligand. High-throughput protein crystallography was used as the primary method of experimental validation [Figure 3 and Table 1]. It allows for unambiguous identification of weak binders (affinity in millimolar range) and provides important structural information. The binding affinity was quantified by the detection system used in the homogeneous time-resolved fluorescence (HTRF) assay reported previously[18] and for three fragments by isothermal titration calorimetry (ITC). The quantification of binding affinity by the HTRF assay uses a truncated protein (only the 165-residue YTH domain of the YTHDC1 protein which consists of 727 residues) N-terminally tagged with glutathione *S*-transferase. Such an approach is dictated by the fact that the rest of the protein comprises low-complexity sequences that do not contribute directly to m^{6}A binding and complicate the recombinant protein chemistry workflow. Validation by biophysical measurements, ITC measurements, and crystal structures of the complexes (which are techniques orthogonal to HTRF) provide additional evidence of m^{6}A-competitive binding.

Fragments **1** and **2** are analogues of methylated adenine as they both contain a pyrimidine ring and $-NHCH_3$ group. Their binding mode resembles that of the adenine moiety of m^{6}A. Fragment **3** lacks one of the two nitrogen atoms of the pyrimidine. As a result, while the $-NHCH_3$ group binds the aromatic cage and hydrogen-bonds to the Ser378 backbone, compared to fragment **2**, it no longer makes an interaction to Asn367 and the plane of its ring system is rotated by about 40°. When an analogue with the second ring saturated, fragment **4**, was tested, the aliphatic ring system was found in the aromatic cage instead of $-NHCH_3$. Furthermore, the hydrophobic loop, including Leu439 from the hydrophobic cage, is displaced to accommodate the $-NHCH_3$ group. Finally, there is no donating hydrogen bond from the fragment to the backbone of Ser378. Instead, the $-NHCH_3$ group of fragment **4** interacts with the side chain of Ser378 through a mediating water molecule.

Fragment **4** has provided an example of molecule that does not interact with aromatic cage through the -$NHCH_3$ group. We identified further molecules binding to YTH domain of YTHDC1 that lacked this trivial m^{6}A isostere. Fragment **5** comprises a similar aliphatic ring, fused to an uracil moiety. Like fragment **4**, its aliphatic part interacts with the Trp cage, yet the overall conformation of the protein is reminiscent of that binding m^{6}A or fragments **1** and **2**. The uracil moiety forms a hydrogen bond with the backbone carbonyl of Ser378 with the NH group next to the aliphatic ring, while the adjacent carbonyl is involved in water-bridged interactions with the side chain of Asp476. Further exploration of uracil derivatives yielded fragments **6**−**8**. Fragment **6** preserves the key interaction between the aliphatic ring and aromatic cage, as well as the hydrogen bond between uracil moiety NH and Ser378 backbone. As it is longer than **5**, it engages Asp476 as well as Arg404 through uracil's second CONH motif. Fragment **7** features a replacement of the azacyclopentane ring with benzyl, which fits the Trp cage well and is the first example of an aromatic moiety bound to it. The uracil moiety can be replaced with an *N*-carbamoylcarboxyamide moiety, yielding fragment **8** and maintaining the binding mode and much of hydrogen bond network of the molecule.

We then sought to present $-NHCH_3$ to the Trp cage by using the uracil scaffold. In the course of exploring the commercially available derivatives, we have selected *N*,*N*,*N*-trimethylamines, substituted at two methyl groups with uracilyl and another aromatic group, respectively. The compounds **9** and **10** reproduced the binding mode of the uracil moiety of

https://dx.doi.org/10.1021/acschembio.9b00894
ACS Chem. Biol. 2020, 15, 618−625

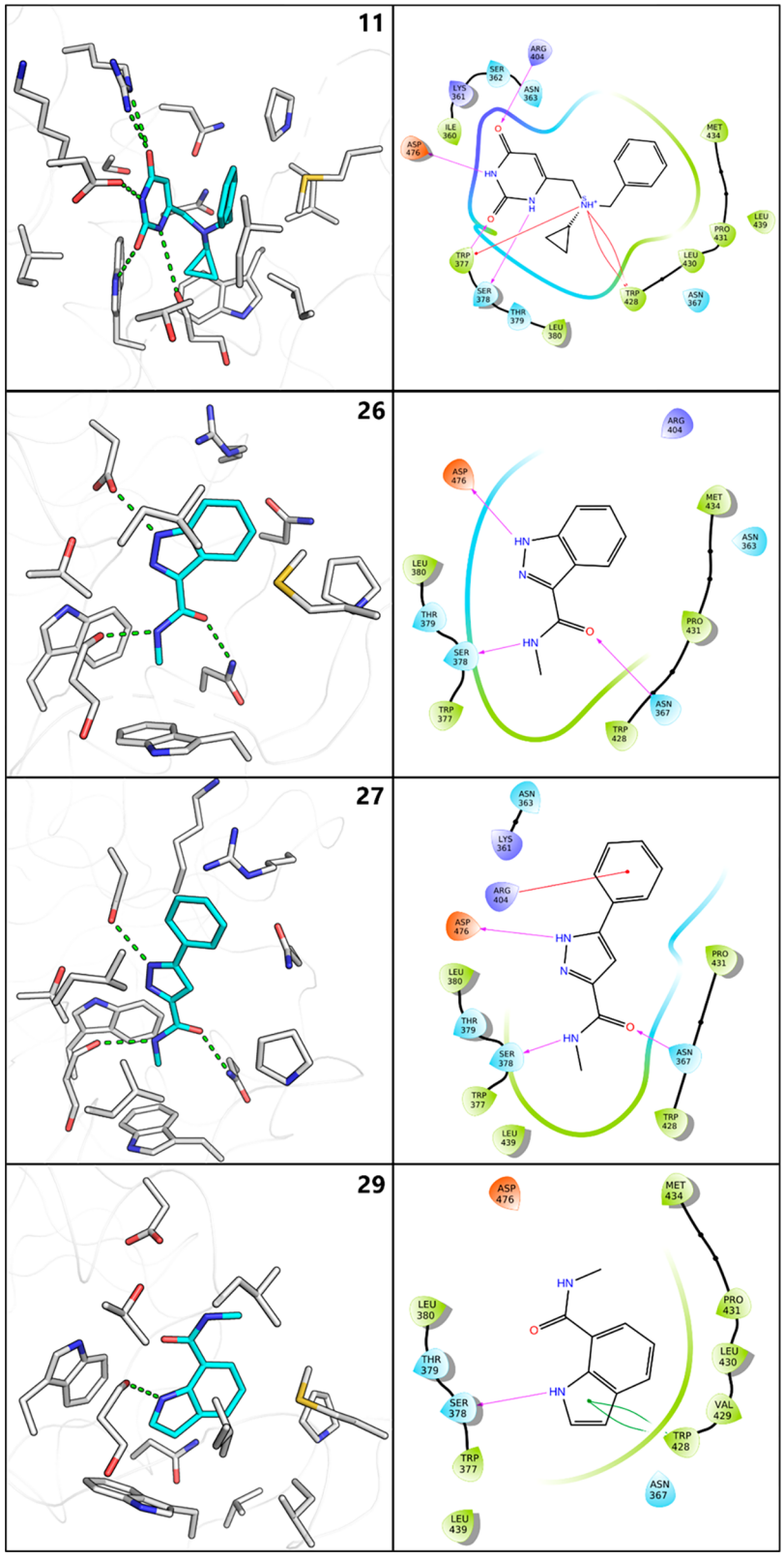

Figure 3. (Left) Crystal structures and (right) two-dimensional projections (Maestro, Schrödinger, LLC, New York, NY, 2019) of the complexes between the m^{6}A-reader domain of YTHDC1 and sub-millimolar fragments with good ligand efficiency, namely, compounds **11**, **26**, **27**, and **29** (from top to bottom). The hydrogen bonds are shown by green dashed lines (left) and magenta arrows (right).

fragments **6** and **7**, and the binding of the $-NHCH_3$ group in m^{6}A (and fragments **1** and **2**), as shown by crystallographic analysis. The second aromatic ring (phenyl in **9** or 3-thienyl in **10**) has lined against the hydrophobic loop, filling the rest of the pocket and also forming an intraligand $\pi-\pi$ sandwich-like stacking interaction with the uracil moiety. Interestingly, by replacing the *N*-methyl group in **9** with *N*-cyclopropyl as in compound **11** [Figure 3, top], the van der Waals interactions

https://dx.doi.org/10.1021/acschembio.9b00894
ACS Chem. Biol. 2020, 15, 618−625

Table 1. Thirty Fragments That Bind to the m^{6}A Reader Domain of YTHDC1 According to Protein Crystallography[a]

Cpd	2D Structure	IC_{50} [μM]	LE	PDB ID (Res.)
1	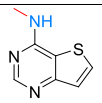	>1000	-	6SYZ (2.28)
2		>1000	-	6SZ1 (1.74)
3	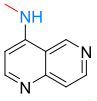	ND*	-	6SZ2 (1.52)
4	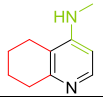	ND*	-	6SZ3 (1.28)
5	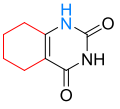	1615	0.32	6SZ7 (2.31)
6	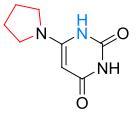	>1000	-	6SZ8 (1.46)
7	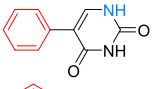	>1000	-	6SZL (1.45)
8	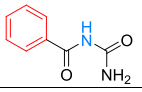	>1000	-	6SZN (1.47)
9	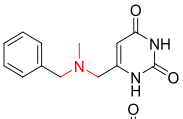	>1000	-	6SZR (1.64)
10	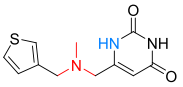	1926	0.22	6SZT (1.5)
11	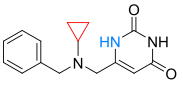	228	0.25	6SZX (1.17)
12	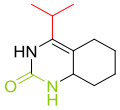	>1000	-	6SZY (1.79)
13	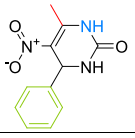	2057	0.22	6T01 (1.5)
14	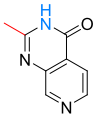	>1000	-	6T0O (1.71)

Cpd	2D Structure	IC_{50} [μM]	LE	PDB ID (Res.)
15	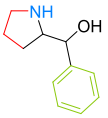	>1000	-	6T02 (1.1)
16		>1000	-	6T03 (1.5)
17	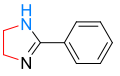	>1000	-	6T04 (1.5)
18	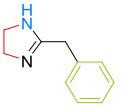	>1000	-	6T05 (1.5)
19	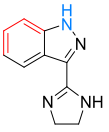	2010	0.26	6T06 (2.4)
20	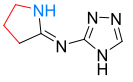	>1000	-	6T07 (1.5)
21	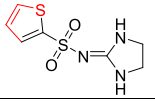	>1000	-	6T08 (1.41)
22	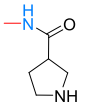	>1000	-	6T0X (1.36)
23	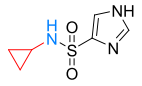	>1000	-	6T0Z (1.43)
24	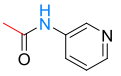	>1000	-	6T09 (1.75)
25	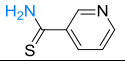	2040	0.41	6T0A (2.02)
26	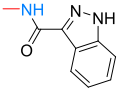	155	0.40	6T0C (2.03)
27	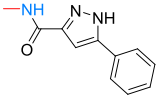	391	0.31	6T0D (1.43)
28	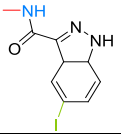	348	0.34	6T10 (1.48)
29	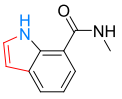	402	0.36	6T11 (1.49)
30	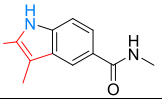	825	0.28	6T12 (1.46)

[a]The colors in the 2D structures indicate a hydrogen bond donor to the backbone carbonyl oxygen of Ser378 (blue), carbon atoms in the Trp cage (red), and a moiety that displaces the flexible loop (green). The 30 compounds can be grouped in 10 chemotypes (horizontal lines). The HTRF dose−response curves corresponding to the IC_{50} values are shown in Figure S2. The inhibition constant is approximatively $IC_{50}/2$, since the m^{6}A-containing ribonucleotide (i.e., the natural ligand employed as competitor in the HTRF assay) was used at a concentration close to its K_D value. The K_D value of fragments **11**, **13**, and **26** is 58, 2100, and 22 μM, respectively (ITC data in Table S1). The resolution is in Å. LE = Ligand Efficiency. * The IC50 value could not be measured due to assay interference and/or solubility limit.

https://dx.doi.org/10.1021/acschembio.9b00894
ACS Chem. Biol. 2020, 15, 618−625

in the Trp cage improve, leading to IC_{50} = 228 μM and a dissociation constant K_D = 58 μM as measured by ITC [Figure S1].

Encouraged by the versatility of the uracil scaffold, we explored further closely related bicyclic systems with different substitution patterns. Fragment **12** bound with an isopropyl moiety in the Trp cage and not with an aliphatic ring as, e.g., fragments **4** and **5**. At the same time, there is no hydrogen bond to the backbone carbonyl of Ser378, which is replaced by van der Waals interactions to the central −CH of the isopropyl group, a very unique feature among the YTHDC1 binders. The carbonyl group of fragment **12** makes hydrogen bonds to Asn367 and a proximal water molecule, which positions the fragment in such a way that it slightly displaces the hydrophobic loop. Molecule **13** features a phenyl substituent in the ring and causes a larger rearrangement of the hydrophobic loop than fragment **12**. Fragment **14** recapitulates the binding mode of the methyl and urea groups of fragment **13**, but its ring system is rotated by about 50°.

Based on the knowledge of molecular recognition of the system, we then performed a broader screening campaign to identify further scaffolds that can replace the epitranscriptomic m^6A mark in the Trp cage. Inspired by fragment **6**, we have docked a library of compounds containing five-member (partially) saturated rings with at least one nitrogen atom. We identified a number of molecules containing 4,5-dihydro-2*H*-imidazole-1-yl to be recognized by the Trp cage, including fragments **15**−**21**. The aliphatic five membered ring assumes a fairly conserved pose for the fragments **15**−**18** and **20**, with the nitrogen atom making a hydrogen bond to the main chain carbonyl of Ser378. To accommodate the phenyl ring present in fragments **15** and **18**, the rearrangement of the binding site loop is observed. This is not the case for fragment **17**, in which the phenyl ring is connected directly to a five-membered ring and can be accommodated in the smaller form of the pocket. Fragment **19** is similar to fragment **18**, formally with an additional closed ring. However, for geometry reasons, it cannot maintain the binding mode of **18** and its phenyl ring is seen to occupy the Trp cage, while the nitrogen atom of the double-ring system makes an interaction with the Ser378. The binding of these fragments appears also to be dependent on the presence in the binding pocket of a sulfate ion which originates from the crystallization buffer. Similarly, in the case of compound **21**, the combination of electronic and geometric factors leads to accommodation of the aromatic thiophene ring, rather than the aliphatic nitrogen-containing ring, in the Trp cage. However, in the case of this compound, there is no hydrogen bond to Ser378, which is rare for ligands of YHTDC1. It should be noted that the close analogue **20** binds with aliphatic ring in the Trp cage.

We have also identified a series of substituted amides as versatile isosteres of m^6A modification. Compounds **22** and **23** both bound with their N-aliphatic moieties in the Trp binding pocket and have an amide nitrogen making a hydrogen bond to the main chain of Ser378. The orientation of the oxygen atoms in the amide **22** and sulfonamide **23** differed, with the latter pointing in the direction of the hydrophobic loop and making van der Waals interactions. Compound **24** features an *N*-acetylamide moiety, with the acetyl moiety being recognized by the Trp cage and the amide NH group making a hydrogen bond to the carbonyl of Ser378. The thioamide compound **25** has its sulfur atom next to the side chain NH_2 of Asn367 engaging in a weak polar contact. Its amide nitrogen serves as both the partial positive charge bearer to bind the aromatic cage and the hydrogen bond donor to interact with the backbone of Ser378. The good ligand efficiency of fragment **25** (0.41 kcal/mol per non-hydrogen atom) is quite surprising considering that it does not feature any carbon atom in the Trp cage. Both compounds **24** and **25** contain a pyridine moiety whose nitrogen atom is involved in water-bridged interactions with the side chains of Thr379 and Asp476.

The diazole-containing compounds bearing an *N*-methyl-carbamide substitution are involved in an interesting array of interactions to the side chains of Asp476 and Thr379 in the binding pocket. Compound **26** and **27** are two notable examples, with an additional six-member ring either fused to or connected to diazole by a single bond [Figure 3, middle]. The phenyl ring of compound **27** takes the spot of the ribose ring in m^6A is involved in a previously unobserved π−cation interaction with the side chain of Arg404. Of all the compounds reported here, fragment **26** shows the highest affinity to the protein (IC_{50} = 155 μM and K_D = 22 μM) and has favorable van der Waals interactions with the hydrophobic loop. We have also tested the iodo-derivative of compound **26**, i.e., fragment **28**. The halogen points in the direction of the hydrophobic loop, which caused its rearrangement to accommodate this hydrophobic and large substituent. However, it resulted in a slightly lower affinity and also poor solubility. These two compounds have shown the highest affinities to the protein and good ligand efficiencies. It is noteworthy that fragment **26** has similar affinity to the YTHDC1 reader as the corresponding group of the natural ligand (m^6A, IC_{50} = 144 μM and K_D = 36 μM, Figures S1 and S2) and is more ligand efficient as it is smaller than m^6A (13 and 20 non-hydrogen atoms in **26** and m^6A, respectively).

While this study has revealed the *N*-methyl amides as versatile, easy to introduce and highest affinity binders of the YTHDC1 m^6A binding site, the presence of such a moiety in the molecule does not preclude the binding mode with another group recognized by the Trp cage. In a small set of analogues of **26** and **27**, we have identified compound **29**. The NH of the *N*-methyl amide group of **29** mimics the interaction to the side chains of Asp476 and Thr379 seen for diazole of **26** and **27**, while its indole ring is bound in the Trp cage [Figure 3, bottom]. In another example, the dimethyl substituted pyrrole of the indole ring of **30** is bound at the Trp cage, and its *N*-methyl amide is directed outside of the pocket, toward the solvent. In both compounds **29** and **30**, the indole NH acts as donor in the key hydrogen bond to the backbone carbonyl of Ser378.

To evaluate selectivity against other human m^6A reader domains, 24 of the 30 fragments were tested for binding to one or more of the YTHDF1, YTHDF2, and YTHDF3 readers by the HTRF assay. Significant binding at a concentration of 1 mM was observed only for fragment **26** (Table S2). The dose−response measurements show that fragment **26** has similar affinity for YTHDC1 and YTHDF2 (about 150 μM) and slightly worse affinity for YTHDF1 and YTHDF3 [Figure S2]. Interestingly, fragment **28** which differs from **26** by a single iodine atom does not show measurable binding to the YTHDF1/2/3 reader domains at a concentration of 1 mM which indicates that functionalization of fragment **26** will result in selectivity for YTHDC1. Thus, most fragments are selective for the reader of YTHDC1 and against YTHDF1/2/3. Binding to YTHDC2 was not tested.

https://dx.doi.org/10.1021/acschembio.9b00894
ACS Chem. Biol. 2020, 15, 618−625

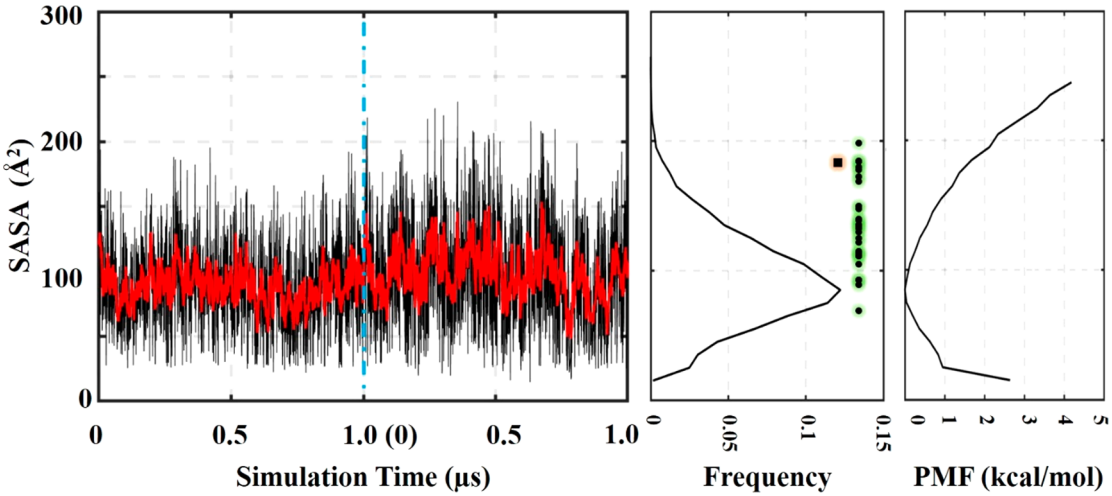

Figure 4. Solvent accessible surface area (SASA) of the m^{6}A binding pocket in the reader domain of YTHDC1. (Left) Time series of SASA along two MD runs of 1 μs each. The black and red lines denote the raw values and running average, respectively. (Middle) Distribution of SASA of the binding pocket from the 2 μs of MD simulations (solid line) and values of the 30 crystal structures of holo YTHDC1 (circles with green halo) and apo YTHDC1 (square with pink halo). (Right) Potential of mean force (PMF) along the SASA of the binding pocket. The PMF is calculated as $-k_BT \ln \frac{p_i}{p_0}$, where k_B is the Boltzmann factor, T is the temperature (300 K), p_i is the population in bin i (bin width of 10 Å^2), and p_0 is the probability of the most populated bin.

The m^{6}A recognition pocket and in particular the binding site loop (residues 429−439) exhibit significant plasticity [Figure 2]. Two methionine side chains (Met434 and Met438) are disordered [Figure 2], and as mentioned above Leu439 changes orientation upon binding of some of the ligands (e.g., fragment **4**). These residues are involved in favorable van der Waals interactions with different ligands in the pocket. Furthermore, the more distal side chain of Arg404 can assume different orientations. In contrast, the side chains of Trp377 and Trp428 are rigid. Molecular dynamics simulations provide evidence that spontaneous fluctuations of the loop in the microsecond time scale result in different apertures of the binding site [Figure 4]. It is interesting to note that the values of the solvent accessible surface area (SASA) of the binding site in the 30 holo structures span a similar range as the one sampled during the simulations [Figure 4, middle]. This overlap suggests a good coverage of conformational space of the binding pocket by the herein described chemical matter.

Our study provides evidence that protein-RNA interactions dependent upon epitranscriptomic modification m^{6}A can be disrupted with small molecules. While interaction of the ligand with the Trp cage as well as the hydrogen bond to the adjacent Ser378 seem to be the key for molecular recognition [Figure 3], they can be achieved using a number of different chemotypes, including both aliphatic and aromatic partially positively charged moieties [Table 1]. The series of *N*-methyl amides has shown particularly good binding affinities and high ligand efficiencies, which gives promise for future development of chemical probes or blockers that can be used in cellular or in vivo studies. In the recently disclosed context of involvement of other YTH domains in cancer, or possible applications of such molecules in cancer combination-immunotherapy, they are likely to attract further attention of the drug discovery community.

Finally, our crystallographic analysis has unveiled several unexpected changes in the binding mode upon relatively small structural changes in the binding site. Although YTH domains were annotated as m^{6}A binders, they seem to be more promiscuous as originally described and able to also bind other small molecules in the cells or transcripts bearing different modifications. Of note, there have been preliminary reports that YTH readers may also recognize m^{1}A modifications.[19] With more than 100 low-abundance modifications present in the transcriptome, further discoveries of specific molecular recognition events are contingent upon improvement in detection methodologies. It should be noted that bromodomains, readers of lysine acetylation modifications, have been shown recently to also recognize other modifications, e.g., crotonylation.[20] It cannot be excluded that higher promiscuity will be observed for epitranscriptomic readers in the near future.

■ ASSOCIATED CONTENT

Supporting Information

The Supporting Information is available free of charge at https://pubs.acs.org/doi/10.1021/acschembio.9b00894.

Experimental methods, computational methods for molecular dynamics and binding pocket analysis, ITC curves and thermodynamic parameters, HTRF dose−response curves and single-dose measurements, X-ray data collection and refinement statistics for the 30 crystal structures, electron density maps of fragments, binding mode of the 30 fragments as observed in the crystal structures (PDF)

■ AUTHOR INFORMATION

Corresponding Authors

Amedeo Caflisch − *Department of Biochemistry, University of Zurich, CH-8057 Zurich, Switzerland;* orcid.org/0000-0002-2317-6792; Email: caflisch@bioc.uzh.ch

Pawel Sledz − *Department of Biochemistry, University of Zurich, CH-8057 Zurich, Switzerland;* orcid.org/0000-0002-4440-3253; Email: p.sledz@bioc.uzh.ch

https://dx.doi.org/10.1021/acschembio.9b00894
ACS Chem. Biol. 2020, 15, 618−625

Authors

Rajiv Kumar Bedi − *Department of Biochemistry, University of Zurich, CH-8057 Zurich, Switzerland*

Danzhi Huang − *Department of Biochemistry, University of Zurich, CH-8057 Zurich, Switzerland*

Lars Wiedmer − *Department of Biochemistry, University of Zurich, CH-8057 Zurich, Switzerland*

Yaozong Li − *Department of Biochemistry, University of Zurich, CH-8057 Zurich, Switzerland;* orcid.org/0000-0002-5796-2644

Aymeric Dolbois − *Department of Biochemistry, University of Zurich, CH-8057 Zurich, Switzerland*

Justyna Aleksandra Wojdyla − *Swiss Light Source, Paul Scherrer Institute, 5232 Villigen, Switzerland*

May Elizabeth Sharpe − *Swiss Light Source, Paul Scherrer Institute, 5232 Villigen, Switzerland*

Complete contact information is available at: https://pubs.acs.org/10.1021/acschembio.9b00894

Funding

Swiss National Science Foundation Grant No. 310030B-189363 to A.C. Entrepreneur Fellowship in Biotechnology (BIOEF-18-008) from UZH Foundation and grant from the Swiss Innovation Agency Innosuisse to P.S. An International Postdoc Grant funded by the Swedish Research Council (VR 2019-00608) to Y.L.

Notes

The authors declare no competing financial interest.

PDB accession codes of the structures of the YTHDC1 in complex with fragments are **1** (6SYZ), **2** (6SZ1), **3** (6SZ2), **4** (6SZ3), **5** (6SZ7), **6** (6SZ8), **7** (6SZL), **8** (6SZN), **9** (6SZR), **10** (6SZT), **11** (6SZX), **12** (6SZY), **13** (6T01), **14** (6T0O), **15** (6T02), **16** (6T03), **17** (6T04), **18** (6T05), **19** (6T06), **20** (6T07), **21** (6T08), **22** (6T0X), **23** (6T0Z), **24** (6T09), **25** (6T0A), **26** (6T0C), **27** (6T0D), **28** (6T10), **29** (6T11), **30** (6T12).

■ ACKNOWLEDGMENTS

We thank the staff at X06DA beamline, Swiss Light Source, Paul Scherrer Institute (Villigen, Switzerland) for assistance in data collection.

■ REFERENCES

(1) Seiler, M., Yoshimi, A., Darman, R., Chan, B., Keaney, G., Thomas, M., Agrawal, A. A., Caleb, B., Csibi, A., Sean, E., Fekkes, P., Karr, C., Klimek, V., Lai, G., Lee, L., Kumar, P., Lee, S. C., Liu, X., Mackenzie, C., Meeske, C., Mizui, Y., Padron, E., Park, E., Pazolli, E., Peng, S., Prajapati, S., Taylor, J., Teng, T., Wang, J., Warmuth, M., Yao, H., Yu, L., Zhu, P., Abdel-Wahab, O., Smith, P. G., and Buonamici, S. (2018) H3B-8800, an orally available small-molecule splicing modulator, induces lethality in spliceosome-mutant cancers. *Nat. Med. 24*, 497−504.

(2) Connelly, C. M., Moon, M. H., and Schneekloth, J. S., Jr. (2016) The Emerging Role of RNA as a Therapeutic Target for Small Molecules. *Cell Chem. Biol. 23*, 1077−1090.

(3) Shi, H., Wei, J., and He, C. (2019) Where, When, and How: Context-Dependent Functions of RNA Methylation Writers, Readers, and Erasers. *Mol. Cell 74*, 640−650.

(4) Boriack-Sjodin, P. A., Ribich, S., and Copeland, R. A. (2018) RNA-modifying proteins as anticancer drug targets. *Nat. Rev. Drug Discovery 17*, 435−453.

(5) Lin, S., Choe, J., Du, P., Triboulet, R., and Gregory, R. I. (2016) The m(6)A Methyltransferase METTL3 Promotes Translation in Human Cancer Cells. *Mol. Cell 62*, 335−345.

(6) Li, Y., Bedi, R. K., Wiedmer, L., Huang, D., Sledz, P., and Caflisch, A. (2019) Flexible Binding of m(6)A Reader Protein YTHDC1 to Its Preferred RNA Motif. *J. Chem. Theory Comput. 15*, 7004−7014.

(7) Wang, X., and He, C. (2014) Reading RNA methylation codes through methyl-specific binding proteins. *RNA Biol. 11*, 669−672.

(8) Patil, D. P., Pickering, B. F., and Jaffrey, S. R. (2018) Reading m(6)A in the Transcriptome: m(6)A-Binding Proteins. *Trends Cell Biol. 28*, 113−127.

(9) Cochran, A. G., Conery, A. R., and Sims, R. J., 3rd (2019) Bromodomains: a new target class for drug development. *Nat. Rev. Drug Discovery 18*, 609−628.

(10) Liao, S., Sun, H., and Xu, C. (2018) YTH Domain: A Family of N(6)-methyladenosine (m(6)A) Readers. *Genomics, Proteomics Bioinf. 16*, 99−107.

(11) Xu, C., Wang, X., Liu, K., Roundtree, I. A., Tempel, W., Li, Y., Lu, Z., He, C., and Min, J. (2014) Structural basis for selective binding of m6A RNA by the YTHDC1 YTH domain. *Nat. Chem. Biol. 10*, 927−929.

(12) Majeux, N., Scarsi, M., Apostolakis, J., Ehrhardt, C., and Caflisch, A. (1999) Exhaustive docking of molecular fragments with electrostatic solvation. *Proteins: Struct., Funct., Genet. 37*, 88−105.

(13) Majeux, N., Scarsi, M., and Caflisch, A. (2001) Efficient electrostatic solvation model for protein-fragment docking. *Proteins: Struct., Funct., Genet. 42*, 256−268.

(14) Zhao, H., and Huang, D. (2011) Hydrogen bonding penalty upon ligand binding. *PLoS One 6*, No. e19923.

(15) Marchand, J. R., and Caflisch, A. (2018) In silico fragment-based drug design with SEED. *Eur. J. Med. Chem. 156*, 907−917.

(16) Sledz, P., and Caflisch, A. (2018) Protein structure-based drug design: from docking to molecular dynamics. *Curr. Opin. Struct. Biol. 48*, 93−102.

(17) Morris, G. M., Huey, R., Lindstrom, W., Sanner, M. F., Belew, R. K., Goodsell, D. S., and Olson, A. J. (2009) AutoDock4 and AutoDockTools4: Automated docking with selective receptor flexibility. *J. Comput. Chem. 30*, 2785−2791.

(18) Wiedmer, L., Eberle, S. A., Bedi, R. K., Sledz, P., and Caflisch, A. (2019) A Reader-Based Assay for m(6)A Writers and Erasers. *Anal. Chem. 91*, 3078−3084.

(19) Dai, X., Wang, T., Gonzalez, G., and Wang, Y. (2018) Identification of YTH Domain-Containing Proteins as the Readers for N1-Methyladenosine in RNA. *Anal. Chem. 90*, 6380−6384.

(20) Flynn, E. M., Huang, O. W., Poy, F., Oppikofer, M., Bellon, S. F., Tang, Y., and Cochran, A. G. (2015) A Subset of Human Bromodomains Recognizes Butyryllysine and Crotonyllysine Histone Peptide Modifications. *Structure 23*, 1801−1814.